This is the preprint version of the contribution published as:

Guo, F., Wu, Q., **Schlink, U.** (2021):
3D building configuration as the driver of diurnal and nocturnal land surface temperatures: Application in Beijing's old city
Build. Environ. **206** , art. 108354

The publisher's version is available at:

https://doi.org/10.1016/j.buildenv.2021.108354

3D building configuration as the driver of diurnal and nocturnal land surface temperatures: application in Beijing's old city

Fengxiang Guo (Corresponding author)

Affiliation: Department of Urban and Environmental Sociology, UFZ-Helmholtz Centre for Environmental Research, Germany

E-mail address: fengxiang.guo@ufz.de

Postal address: Permoserstraße 15, 04318 Leipzig, Germany

Phone number: 0049 176 6864 3237

Fax number: 0049 341/235 45 1554

Qiong Wu

Affiliation: College of Geo-Exploration Science and Technology, Jilin University, China

E-mail address: wuqiong@jlu.edu.cn

Uwe Schlink

Affiliation: Department of Urban and Environmental Sociology, UFZ-Helmholtz Centre for Environmental Research, Germany

E-mail address: uwe.schlink@ufz.de

Abstract

Urbanization has produced extremely diverse structures of buildings, including horizontal sprawl, vertical growth, and a transition from traditional to modern architecture. Although the influence of urban morphology on urban heat formation is unquestioned, previous research has relied just on the 2D building composition and its influence on diurnal land surface temperatures (DLSTs). However, it is not well known that the 3D building configuration affects nocturnal land surface temperatures (NLSTs) and seasonal variations. In a new approach, a set of 3D landscape metrics, based on both aspects of composition and configuration, is here proposed and tested for spatiotemporal associations to land surface temperatures (LSTs) in Beijing's old city. The combination of classical and modern architecture styles makes this region an ideal laboratory for LST studies in highly different urban structures. Major findings include: 1) 3D landscape metrics effectively and suitably describe the diversity, irregularity and spatial arrangement of buildings; 2) Denser and more compact building patterns result in higher DLSTs, whereas highest NLSTs occur around modern high-rise buildings; 3) 3D landscape metrics have sensitive correlations to DLSTs, but in general NLSTs are closer associated with composition metrics rather than configuration metrics; 4) Both DLST and NLST are most importantly affected by building numbers and nearest distances between buildings; 5) The association between urban morphology and LSTs is fairly stable over all four seasons; with the variation that the summer relationship was relatively lower due to stronger solar radiation and evapotranspiration of urban vegetation.

Keyword: 3D landscape metrics, urban building patterns, land surface temperature, multiple building styles, urban morphology

1. Introduction

Urbanization is one of the most significant human activities since the 20th century, and lots of buildings have been built, remodeled and enlarged, which affects the urban heat environment significantly (United States Environmental Protection Agency, 2006; Chun and Guldmann, 2014; He et al., 2020). Buildings can alter the reflection and absorption of solar radiation, as well as the proliferation of heat in urban area (Huang and Wang, 2019). The surface roughness and irregularity caused by different height, arrangement and density of buildings lead to location dependent and time dependent temperature variations (Ng et al., 2012; Guo et al., 2016; Wang et al., 2017). Elevated urban temperatures can threaten the health of city dwellers and the living condition of flora and fauna (Voogt and Oke, 2003; Patz et al., 2005; Guo et al., 2020). Therefore, it is important for future urban planning and management to determine how building patterns influence temperatures in cities.

Satellite remote sensing provides up-to-date and spatially explicit land surface temperatures (LSTs) with higher spatial coverage than *in situ* observations that are limited by low-density monitoring networks and uncertain observation accuracy (Ma et al., 2016; Berger et al., 2017). Remote sensing imagery is increasingly used in the literature to identify the spatiotemporal influences of urban buildings on urban heat (Ng et al., 2012; Guo et al., 2016; Wang et al., 2017). A weakness with these studies is that they mainly focused on the diurnal influence of buildings on LSTs on a specific date, while the nocturnal relationship and seasonal variations were rarely considered. The nocturnal temperature is highly related to the human comfort, and might arouse more power consumption for cooling, which in turn, raises air pollution and greenhouse gas emissions (Salamanca et al., 2014). Despite the undisputed importance of 3D spatial structures on LSTs, a comprehensive understanding and explanation are still lacking. Previous studies mostly relied on the two-dimensional (2D) features and three-dimensional (3D) vertical features of buildings (e.g., buildings height, volume, and 3D surface area), rather than 3D spatial configuration. In this study, the characteristics of spatial configuration mainly refer to the compactness and arrangement irregularity of buildings. A compact building structure is usually designed to meet the basic housing requirements for increasing urban population and ease up the conflicts between built-up land and other land use as much as possible (Jim and Chen, 2010; Chun and Guldmann, 2014). Building irregularity is originated from the complexity of single and multiple buildings, and the combination type of building arrangements is directly related to the heat accumulation or heat removal by affecting the urban ventilation, radiation balance schemes, and sunshine conditions (Chun and Guldmann, 2014). Compared with the composition characteristics, the method for measuring configuration of urban building patterns in 3D space is less targeted and systematic, and particularly lacks a complexity evaluation of building arrangements (Jhaldiyal et al., 2018; Kedron et al., 2019).

Metrics for pattern recognition have been widely applied to provide more accurate ecological interpretations for the influence of land use/cover changes on LSTs during past decades (Ma et al., 2016; Wang et al., 2017; Guo et al., 2020; Yu et al., 2020). Traditional landscape metrics are usually calculated in 2D space without 3D vertical information, while the urban buildings actually refer to a 2.5D or 3D representation (Hoechstetter et al., 2008; Wu et al., 2017). Thanks to the progress in 3D information extraction technology (e.g., SAR, LiDAR, and oblique photogrammetry), several 3D landscape pattern metrics have been introduced by combining traditional 2D landscape metrics with 3D vertical features (Frazier and Kedron, 2017; Wu et al., 2017; Kedron et al., 2018). 3D landscape analysis has the advantage of incorporating internal heterogeneity within patches into the calculation and avoids the shortcoming of considering a patch as totally homogeneous in 2D space (Hoechstetter et al., 2008; Frazier and Kedron, 2017). However, these new metrics are rarely considered in describing the spatial configuration and composition of urban building patterns, and their efficiency and suitability are also uncertain. Before applying these new metrics to associate the urban buildings with LST, the following scientific questions need to be solved: 1) How to define the concept ‘patch’ and ‘class’ in building patterns, considering that landscape metrics are usually calculated based on a patch-mosaic model? 2) How to interpret the ecological significance of these new metrics and what building characteristics can they reflect? 3) Which landscape metrics are more sensitive to the correlation between urban building morphology and LSTs?

The originality of our approach is the incorporation of 3D urban morphology (composition and configuration of buildings) into studies of LSTs. During daytime, the landscape characteristics (Wu, 2004; McGarigal et al. 2009) in a high-rise building region might lead to less sky visibility and less direct solar radiation, which is conducive to a mitigation of high LSTs (Huang and Wang, 2019). At night, the buildings replace the sun in warming the surrounding areas. 3D features of buildings might affect the intensity and spatial variations of heat (Geros et al., 2005), and a 3D analysis of the built landscape can quantify and compare the heat release at night and heat storage during daytime.

This paper aims to investigate the relationships between the 3D structure of buildings and LSTs and the main objectives include:

- An evaluation of the effectiveness and suitability of a 3D landscape analysis for studying the spatial heterogeneity of urban building patterns, and its relevance to variations of LSTs.
- The identification of diurnal and nocturnal impacts of urban buildings on the urban thermal environment during the four seasons.

To this end, the experimental setup of this study included 14 remote sensing images over four seasons for extracting land surface temperatures, and 3D geographical data of Beijing's old city. The results can contribute to a deeper understanding of the influence of urban morphology on urban heat and provide suggestions for the management and conservation of traditional buildings and the old city from the perspective of urban heat management.

2. Study Area and Data

2.1. Study area

Beijing is one of the largest cities in the world, covers approximately 16000 km^2 with more than 20 million urban permanent populations. Beijing has been built as a city

3000 years ago, and taken as the national political center for 800 years. Beijing has a humid continental monsoon climate with severe, dry winters, hot summers and strong seasonality (Köppen-Geiger climate class Dwa = humid boreal climate, 593 mm yearly precipitation, 11.9 °C annual mean temperature, maximum temperature up to 40 °C, minimum temperature falling to - 20°C) in the North Temperate Zone. Our study area focuses on Beijing's old city, located at the center of the metropolitan area (latitude 39˚54′N, longitude 116˚23′E), covering a total area of about 40 km^2 (Fig. 1), and comprising lots of royal architecture buildings and local-style dwelling houses (e.g., courtyard houses) with low building height and high-dense distribution. Generally, a courtyard house consists of several single buildings.

Since 1950s, giant changes of building styles have been witnessed, including the introduction of high-rise buildings along the Second Ring Road and the demolition of partial courtyard houses due to the old city conservation and renewal policy (Fig. 1). The royal buildings, courtyard houses and modern buildings shape the typical multiple-building landscape in Beijing's old city compared with outside areas, where the buildings are mainly modern high-rise buildings. The complex building pattern in Beijing's old city is an ideal laboratory for the studies of LSTs in highly different urban structures, which might supply new aspects for strategies balancing between the economic development and culture protection during urbanization.

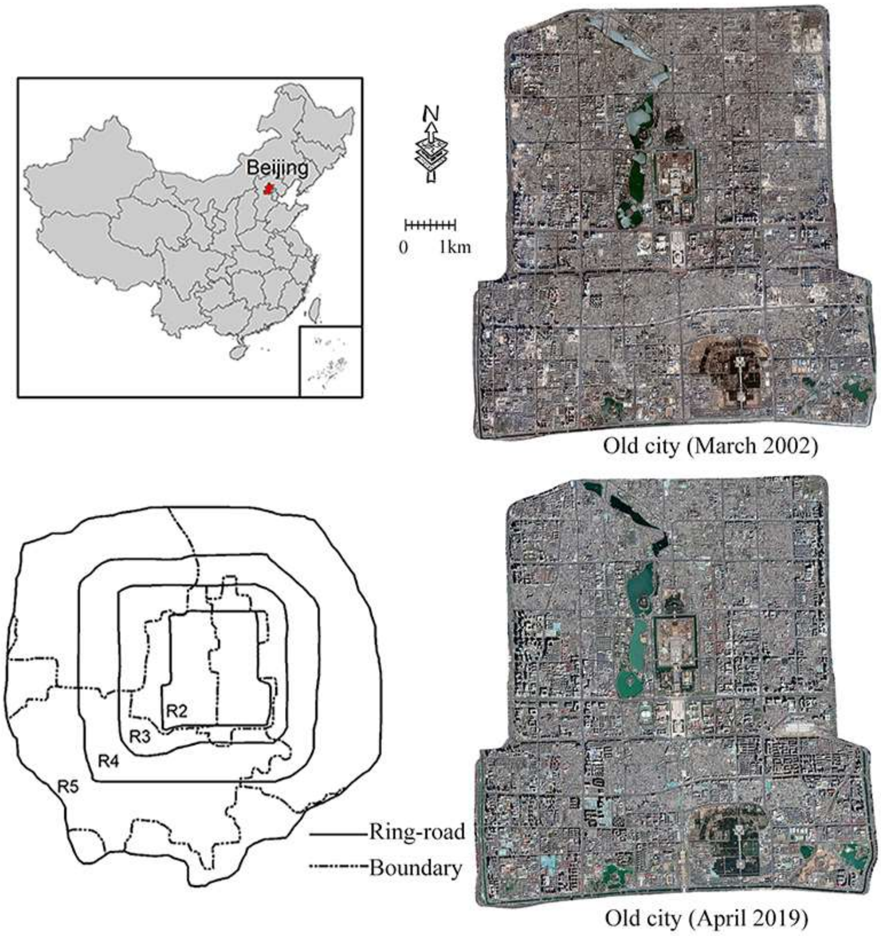

Fig. 1. Study area (top-left corner: map of China; bottom-left corner: the location of main ring roads in Beijing and the old city is surrounded by Second Ring Road (R2); middle: Beijing's old city in March 2002 from Google Earth; right: Beijing's old city in April 2019 from Google Earth).

To test the effectiveness and suitability of 3D landscape metrics in measuring urban building patterns, three samples were chosen according to the following standards: building height, building arrangement regularity, and buildings styles. Generally, urban buildings with modern style are moderate-rise or high-rise and designed with regular arrangement, while urban buildings of traditional styles tend to be low-rise and the spatial arrangement is a little irregular, particularly for the courtyard houses, which have been built over many years. Sample 1 (near Beijing's Drum Tower) mainly consists of courtyard houses (low height and high density of buildings); Sample 2 (near Beijing's railway station) mainly consists of residences with moderate building height and building density; Sample 3 (near central business district) mainly consists of high-rise buildings with relatively scattered spatial distribution of buildings (Fig. 2).

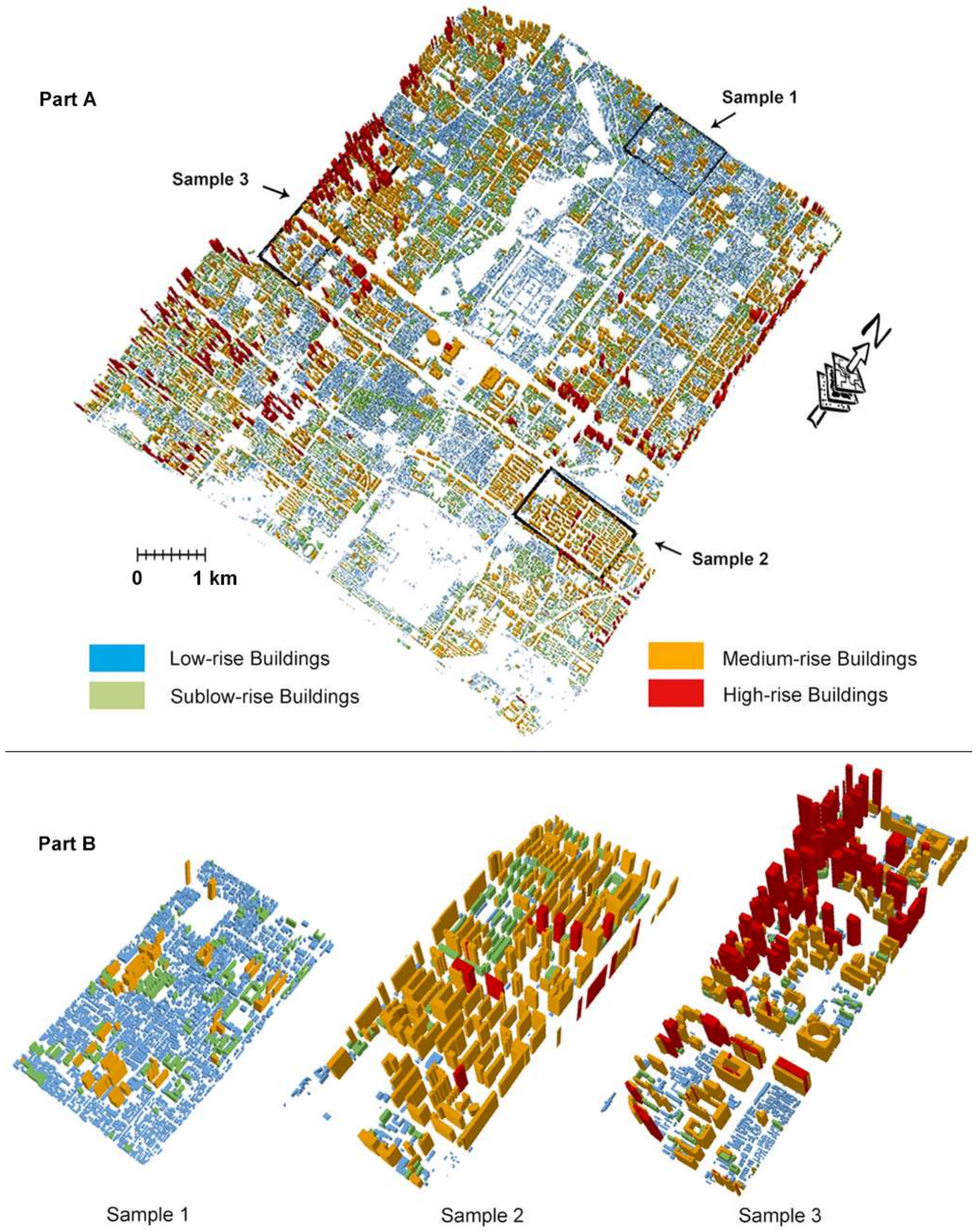

Fig. 2. The building classes in the study area and the location of three selected sample regions (Part A). The standard of buildings classification is seen in Section 3.1. The spatial distribution of buildings in the selected sample regions (Part B).

2.2. Data

For this study, satellite-based remote sensing images from Landsat 8 and Terra were downloaded from the USGS (https://earthexplorer.usgs.gov/) to retrieve LSTs over four seasons at a fine scale (Table 1). 7 Landsat 8 images with Thermal Infrared Sensor (TIRS) were used for the DLST inversion, while 7 Terra images with Advanced

Spaceborne Thermal Emission and Reflection Radiometer (ASTER) were used for the NLST inversion. The accuracy of LST products from Landsat 8 and ASTER might be 1K under better atmospheric correction (Gillespie et al., 1999; Jiménez-Muñoz et al., 2014; Berger et al., 2017), and significant positive relationships existed between inversed and measured temperatures on the weather station (Tiangco et al., 2008; Li et al., 2013). 3D building data were gathered from Baidu China Co., Ltd in 2016, which includes the building footprints and heights (Table 1). All data and remote sensing images were geometrically corrected to the WGS84 coordinate system.

Table 1. Data Sources

Data sources	Data	Local time	Component-derived	Spatial resolution
Landsat 8 OLI/ TIRS	21 Jan 2019	10:53	Diurnal land surface temperature	30 Meter
	26 Mar 2019	10:52		
	13 May 2019	10:52		
	17 Aug 2019	10:53		
	02 Sep 2019	10:53		
	20 Oct 2019	10:53		
	04 Dec 2018	10:53		
Terra ASTER	13 Jan 2019	22:16	Nocturnal land surface temperature	30 Meter
	04 Apr 2011	22:21		
	19 Aug 2017	22:16		
	01 Sep 2019	22:22		
	08 Oct 2015	22:22		
	02 Nov 2015	22:16		
	22 Dec 2016	22:16		
Building data	2016		Building height and footprint	

3. Methods

The data processing consists of three steps (Fig. 3): 1) 3D landscape metrics were calculated based on the footprint and height characteristics of buildings; 2) The DLST and NLST were retrieved using Landsat 8 OLI/TIRS and Terra ASTER remote sensing images, respectively; 3) the diurnal and nocturnal associations between 3D landscape metrics and LSTs were calculated using Pearson correlation coefficient, and their relative importance on affecting the LSTs was evaluated by the random forest algorithm (RF).

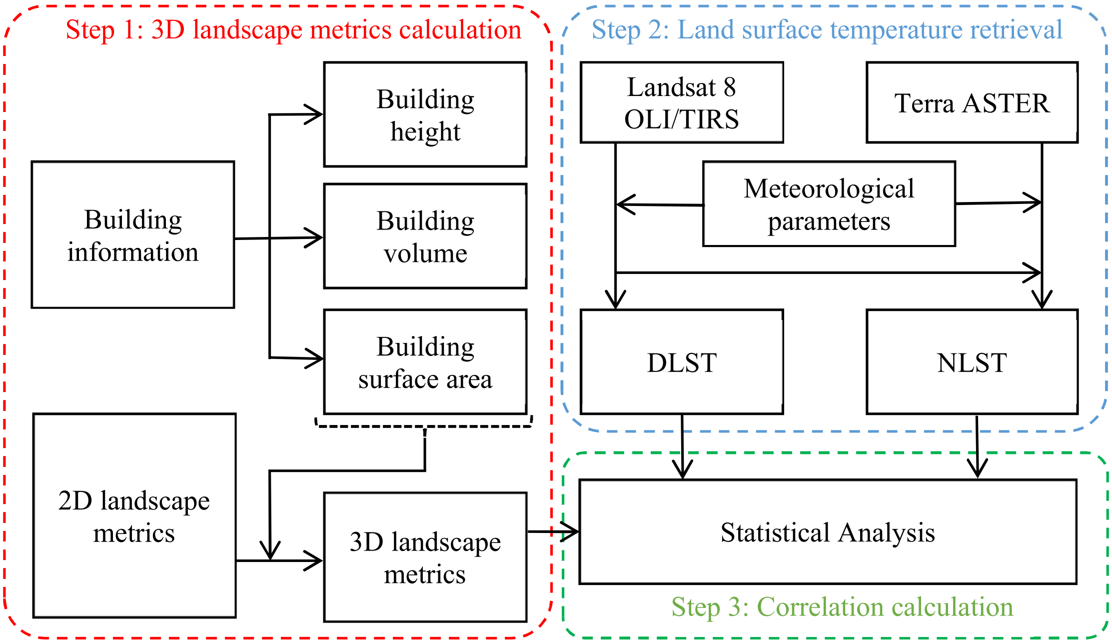

Fig. 3. Flow chart of the implementation and analysing methods.

3.1. Computation of 3D Landscape metrics

The concept 'pattern' in landscape ecology is usually defined based on a patch-mosaic model, which describes the landscape as a mosaic of discrete land use/cover types with certain boundary condition (McGarigal et al., 2009; Frazier and Kedron, 2017; Frazier, 2019). Similarly, an urban building pattern can be seen as a mixture of multiple buildings within a certain area in 3D space (Wu et al., 2017; Frazier, 2019; Kedron et al., 2019). Four levels of heterogeneity are defined to analyze the characteristics of spatial composition and configuration in a building pattern: cell, patch, class, and landscape. The 'cell' is defined as single pixel belonging to urban buildings; the 'patch' is defined as individual 3D building; the 'class' is defined as the mixture of different buildings with the same or similar buildings height; the 'landscape' is defined as the mixture of buildings in the total study area. In this research, we adopted a new set of 3D landscape metrics (composition metrics and configuration metrics) to characterize the complexity, compactness and spatial arrangement regularity of urban buildings (Table 2). The composition metrics are further divided into horizontal and vertical metrics depending on whether 3D vertical landscape elements were put into calculation. The building landscapes were classified into four classes: low buildings (below 10m), sublow-rise buildings (10m-20m), middle-rise buildings (20m-60m), and high-rise buildings (over 60m). The selected 3D landscape metrics were computed using moving window methods with window size 200 m on the MATLAB platform (for full equations and relative description of landscape metrics see supplementary files).

Table 2. Abbreviations and ecological significances of selected 3D landscape metrics.

Metrics	Abbreviation	Type	Measure of the …
Number of patches	NP	Composition-Horizontal	number of urban buildings belonging to the same class.
Patch density	PD	Composition-Horizontal	spatial heterogeneity and evenness of urban building pattern.
Richness density	RD	Composition-Horizontal	richness of urban buildings class within a certain area.
Mean Height	H_{MN}	Composition-Vertical	mean height of urban buildings.
Mean Volume index	V_{MN}	Composition-Vertical	mean volume of urban buildings.
Root-mean-square deviation of height	SQ	Composition-Vertical	undulation of the urban buildings surface.
Percentage of patch type	PLAND	Composition-Vertical	proportion of each buildings class in the urban building pattern.
Largest patch index	LPI	Configuration	largest space occupation of single building.
Simpson's evenness index	SIEI	Configuration	evenness of urban buildings landscape.
Simpson's diversity index	SIDI	Configuration	diversity of urban buildings landscape.
Landscape shape index	LSI	Configuration	deviation between patch shape and regular circle or square with same area.
Landscape fractal dimension index	LFI	Configuration	irregularity and complexity of urban buildings landscape shape.
Landscape division index	LDI	Configuration	fragmentation and aggregation of urban buildings landscape.
Cohesion index	COI	Configuration	connectivity and aggregation of the urban building pattern.
Euclidean nearest-neighbor Mean Distance	ENN	Configuration	isolation degree of each buildings class, and can be taken as indicator for measuring the road width.
Contact index	CNI	Configuration	effect of buildings forming ventilation paths, defined by the ratio between building height and road width (H/W)
Sky view factor	SVF	Configuration	sky visibility

3.2. The land surface temperature retrieval

Current image processing methods for LST retrieval include the mono-window as well as split-window algorithms, single-channel, multi-channel, and atmospheric correct methods (Qin et al., 2001; Berger et al., 2017; Yu et al., 2020). This study applied the mono-window algorithm, which is proposed by Qin et al. (2001) aiming at LST retrieval from only a single thermal infrared band of remote sensing images.

The DLST was retrieved from Landsat 8 images using the radiative transfer model:

$$L_\lambda = L_\mu + \tau[\varepsilon L_T + (1 - \varepsilon)L_d], \tag{1}$$

where L_λ is the at-sensor radiance value; ε is the land surface emissivity; L_μ and L_d are the upwelling and downwelling radiances, respectively; L_T is the black-body radiance given by Planck's law, also known as surface-leaving radiance; τ is the total atmospheric transmissivity between sensor and surface. The atmosphere parameter τ, upwelling radiance L_μ, and downwelling radiance L_d can be calculated using a web-based atmospheric correction parameter tool (https://atmcorr.gsfc.nasa.gov/). The Normalized Difference Vegetation Index (NDVI) can differentiate between vegetated and urban areas based on the continuous values of vegetation abundance, and was applied to calculate the land surface emissivity ε as follows:

$$\varepsilon = 0.02644F_v + 0.96356, \tag{2}$$

where F_v represents the vegetation fraction as expressed in Equation 3:

$$F_V = \left(\frac{NDVI - NDVI_{min}}{NDVI_{max} - NDVI_{min}}\right)^2, \tag{3}$$

and $NDVI$ was calculated by:

$$NDVI = \frac{R_{NIR} - R_{RED}}{R_{NIR} + R_{RED}}, \tag{4}$$

where $NDVI_{min}$ and $NDVI_{max}$ represent the minimum and maximum values of NDVI, respectively; R_{NIR} and R_{RED} represent the reflection values of near-infrared and infrared bands, respectively. The NDVI-based method for emissivity calculation has the effect of reducing the pixel size of the thermal data caused by the Landsat 8 OLI for the NDVI estimation with the resolution 30 meter.

Then, the surface-leaving radiance L_T can be calculated using the following formula:

$$L_T = \frac{L_\lambda - L_\mu - \tau(1-\varepsilon)L_d}{\tau\varepsilon}, \tag{5}$$

Assuming that the Earth surface is a black body, the surface-leaving radiance is converted to at-sensor brightness temperature (T_b) by inverting Planck's law:

$$T_b = \frac{K_2}{ln\left(\frac{K_1}{L_T}+1\right)}, \tag{6}$$

where K_1 and K_2 are two calibration constants. For Landsat 8 OLI, $K_1 = 774.8853\ Wm^{-2}sr^{-1}\mu m^{-1}$ and $K_2 = 1321.0789K$.

The actual land surface temperature was calculated using the at-sensor brightness temperature (T_b) value from Equation (6) as follows:

$$LST = \frac{(a(1-C-D) + T_b(b(1-C-D) + C + D) - DT_a}{C} - 273.15 \tag{7}$$

$$C = \varepsilon\tau, \tag{8}$$

$$D = (1-\tau)[1 + (1-\varepsilon)\tau], \tag{9}$$

where T_a represents the atmosphere mean acting temperature; *a* and *b* are constants, and (for temperatures between 0 °C and 70 °C), *a = −67.355351* and *b = 0.458606.* For the NLST retrieval from ASTER images, the conversion formulae are similar with those used for the Landsat 8 images. However, the lack of daytime ASTER remote sensing images makes that the land surface emissivity applied in the radiative transfer model cannot be derived directly from the same sensor type using the NDVI-based approach. Landsat 8 images were applied to supply the emissivity mask for the NLST retrieval. Due to less noise and atmospheric effects (Gillespie et al., 1999; Nichol, 2005), band 13 was selected from five thermal infrared bands for further use (Fig. 4). Higher DLSTs were mainly observed in traditional building regions, while higher NLSTs were mainly distributed around modern buildings and wider roads.

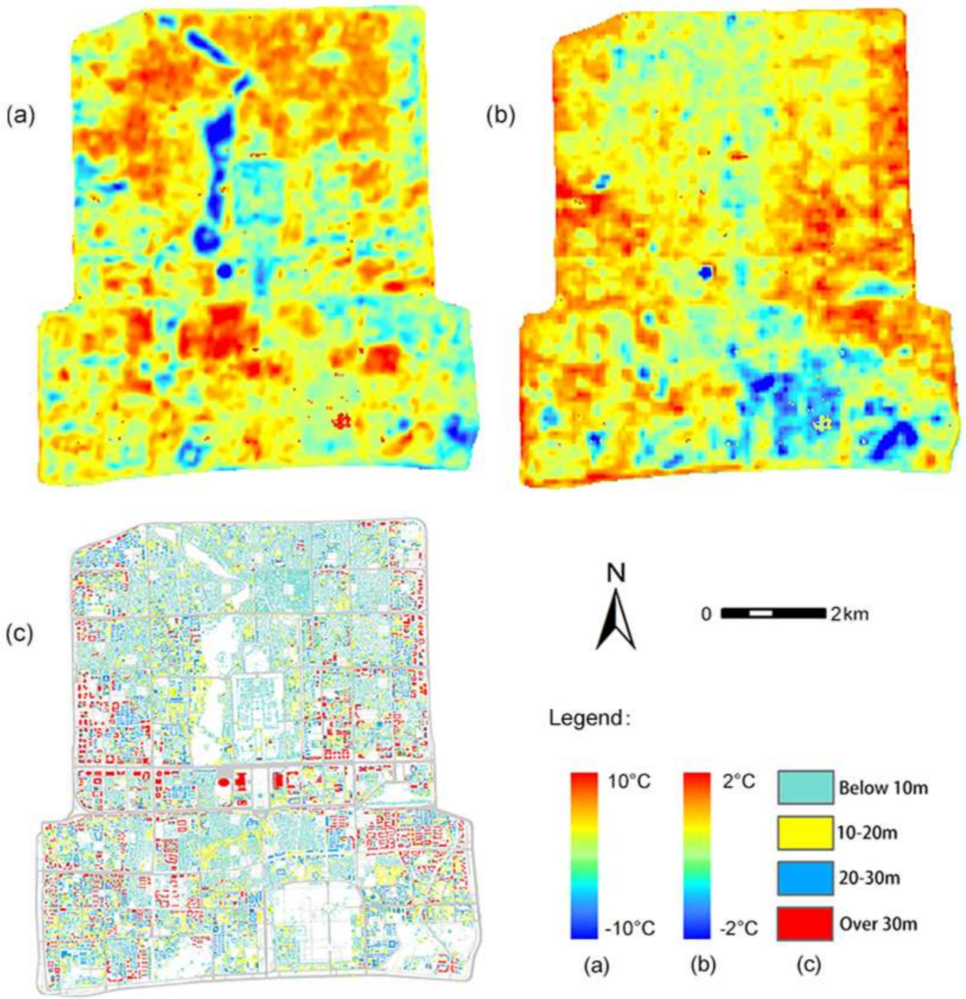

Fig. 4. DLST on January 21, 2019 (a), NLST on January 13, 2019 (b), and building height (c) in Beijing's old city.

3.3. Random forest method evaluating the relative importance of landscape metrics on LSTs

The RF is a nonlinear statistical ensemble algorithm that builds sequential randomised, de-correlated decision trees for classification or regression, and the results are relatively stable for missing or non-stationary data (Hutengs and Vohland, 2016; Xu et al., 2020). RF first generates a training sample through bootstrap resampling, and then forms a random forest of decision trees from the training data. Compared with least-squares linear regression fitting, the advantages of RF are: 1) the inclusion of discrete variables in the regression; 2) nonlinear relationship identification between the predicted and multiple variables; 3) minimised risk of overfitting by averaging a large number of de-correlated individual trees. The relative importance of variables can be calculated from the improvements in split-criterion at each split and in each tree, summing over all variables separately after re-attributing (Hutengs and Vohland, 2016). In this study, we selected 20 3D landscape metrics as the independent variables to predict the diurnal and nocturnal land surface temperatures (regression tree set-up: number of regression trees = 600, minimum number of observations per tree leaf = 5). After training and fitting the RF algorithm, the coefficient of determination (R^2) indicated the accuracy, while the relative importance of variables represented the sensitivity of landscape metrics to the variations of DLST and NLST over four seasons.

4. Results

4.1. 3D landscape metrics for measuring the building patterns in the samples

Significant differences in the building diversity, irregularity and compactness between selected regions were revealed by 3D landscape metrics. In the composition metrics (Table 3), the H_{MN} in Sample 3 (14.301 m) exceeded that in Sample 1 (3.399 m) and Sample 2 (9.707 m) as expected. The NP (1681) and PD (0.005) in Sample 1 were both highest, but the RD (5.977) and volume (1137393 m^3) were lowest, because traditional dwellings-courtyard houses account for the largest proportion in this region, and single buildings belonging to the courtyard house usually take less horizontal space compared with high-rise buildings. In Sample 1, there were no middle-rise and high-rise buildings. With increasing mean height the fraction of low-rise buildings decreased from 0.973 to 0.444. The lowest SQ value (2.336) occurred in Sample 1, because the low-rise buildings usually have less height variations than high-rise region.

Table 3. 3D landscape composition metrics in three samples (classification of the PLAND index: LB - low-rise, SB - sublow-rise, MB - medium-rise, and HB - high-rise buildings.

	H_{MN} (m)	NP	PD	RD	V_{MN} (m^3)	SQ	LB	SB	MB	HB
Sample 1	3.399	1681	0.005	5.977	1137393	2.336	0.973	0.027	0.000	0.000
Sample 2	9.707	301	0.001	6.254	4656600	5.330	0.554	0.435	0.012	0.000
Sample 3	14.301	271	0.001	7.256	7883505	10.369	0.444	0.260	0.169	0.127

In the configuration metrics (Table 4), the LPI in Sample 3 (0.021) was higher than that in Sample 1 (0.015) and Sample 2 (0.018), caused by a larger occupation of horizontal space and larger designed height for single high-rise buildings. The larger SIDI (1.339) and SIEI (0.966) in Sample 3 indicated a much more diverse and relatively even spatial distribution of buildings, and the results of LSI and LFI indicated that the building arrangements in Sample 1 were much more irregular than that in the modern building areas. Nowadays, most of courtyard houses in Beijing's old city are relatively irregularly arranged with poor texture, while modern buildings are follow a certain street planning scheme. A much more subdivided and compact building pattern in Sample 1 was suggested by COI and LDI. The ENN in Sample 3 (16.921 m) exceeded that in sample 1 (9.052 m) and sample 2 (10.751 m), where open building patterns and wider distances among buildings were designed for better lighting conditions, ventilation effects and traffic convenience. Compared with the modern high-rise building region, the traditional houses had larger sky visibility, suggested by the SVF.

Table 4. 3D landscape configuration metrics in three samples.

	LPI	SIEI	SIDI	LSI	LFI	COI	LDI	ENN	CNI	SVF
Sample 1	0.015	0.078	0.054	41.764	3.304	95.387	0.998	9.052	0.386	0.831
Sample 2	0.018	0.642	0.705	24.236	2.302	97.932	0.994	10.751	0.575	0.757
Sample 3	0.021	0.966	1.339	26.508	2.096	98.533	0.992	16.921	0.609	0.785

4.2. The diurnal and nocturnal correlation between composition metrics and LST

Significant correlations between landscape composition metrics and LSTs were identified (Table 5), and the relationship during daytime was opposite from that at night. Except SB and MB, the correlation coefficients of other metrics were significant at the $p=0.05$ level. Among horizontal metrics, NP and PD were positively correlated with DLST, while RD was negatively correlated. Within a certain area, more buildings and higher building density mean more compact building arrangements, leading to lower emissivity and worse ventilation, and then causes a significant increase of DLST. At night, the negative relationship between horizontal metrics and LSTs was directly related to the building styles in Beijing's old city. Based on previous results of our samples, low-rise buildings occupy less horizontal and vertical space than high-rise buildings, but the NLST near the former is much lower than that around latter.

Among vertical metrics, both the H_{MN} and PLAND metrics were negatively correlated with DLST, but positively correlated with NLST. During daytime, the LSTs near high-rise buildings were much lower than that near low-rise buildings, because high-rise buildings might generate more building shadow for cooling. After sunset, the high-rise buildings might release more heat to surrounding environment compared with low-rise buildings, and lead to obvious local high temperature zones. The volume can be the best predictor for revealing the temporal influence of buildings on the LSTs. The nocturnal correlation between volume and LSTs was much more significant than the diurnal correlation, because the volume cannot directly describe the variations of building height, but is the direct parameter for estimating the heat storage during daytime.

Table 5. The diurnal and nocturnal correlation coefficients between composition metrics and LST. Blue and orange suggest higher negative and positive correlations, respectively, while white colour indicates lower correlation.

	Daytime							Night						
	Jan 21	Mar 26	May 13	Aug 17	Sep 02	Oct 20	Dec 04	Jan 13	Apr 04	Aug 19	Sep 01	Oct 08	Nov 02	Dec 22
NP	0.76	0.83	0.77	0.72	0.77	0.74	0.70	-0.27	-0.59	-0.49	-0.31	-0.59	-0.55	-0.51
PD	0.65	0.69	0.59	0.52	0.62	0.63	0.61	-0.43	-0.56	-0.44	-0.40	-0.45	-0.58	-0.48
RD	-0.46	-0.56	-0.60	-0.61	-0.54	-0.46	-0.41	-0.16	0.22	0.24	-0.11	0.36	0.13	0.26
H_{MN}	-0.57	-0.61	-0.47	-0.42	-0.59	-0.60	-0.59	0.69	0.60	0.34	0.44	0.26	0.69	0.42
LB	0.50	0.53	0.36	0.31	0.47	0.50	0.50	-0.58	-0.51	-0.35	-0.39	-0.17	-0.58	-0.45
SB	0.05	0.00	0.04	0.07	0.05	0.07	0.08	-0.03	-0.01	0.12	-0.02	0.04	0.02	0.13
MB	-0.10	-0.11	0.02	0.00	-0.07	-0.09	-0.12	0.19	0.11	0.15	0.15	-0.11	0.09	0.21
HB	-0.59	-0.60	-0.48	-0.43	-0.58	-0.61	-0.61	0.64	0.58	0.28	0.41	0.25	0.66	0.37
SQ	-0.52	-0.56	-0.44	-0.38	-0.57	-0.55	-0.56	0.70	0.57	0.40	0.45	0.28	0.69	0.39
V_{MN}	-0.25	-0.24	-0.07	-0.01	-0.20	-0.27	-0.33	0.67	0.35	0.10	0.34	-0.03	0.48	0.24
	-1							0						+1

4.3. The diurnal and nocturnal correlation between configuration metrics and land surface temperature

Table 6 shows the diurnal and nocturnal correlations between landscape configuration metrics and LSTs. Except the SVF, SIDI and SIEI at night, the correlation coefficients of other metrics were significant at the 0.05 level. Similar to composition metrics, the diurnal and nocturnal correlations were opposite, but the configuration metrics responded better to the DLST than NLST.

LPI was negatively correlated with the DLST, but there was no significant correlation between LPI and NLST. It is caused by the fact that LPI is an indicator for space occupation of largest or highest single buildings, which hardly reflect the total 3D features of buildings in the moving window. The lower coefficients of SIDI and SIEI indicated less sensitivity to describe the impacts of urban buildings on LSTs.

The results of LSI and LFI reflected that a irregular building pattern might generate higher DLST. In Beijing's old city, the regular building pattern is usually planned along the main road for better traffic conditions with the following characteristics: high-rise buildings for saving space and low-density for more sunshine mainly. Compared with irregular building patterns, more regular street patterns and spatial arrangements of buildings might create a better ventilation effect, which is conducive to accelerate the heat removal.

The LDI and COI were significantly correlated with DLST. The former was positive, while the latter was negatively correlated with DLST. Higher LDI and COI indicate a more subdivided and fragmented building pattern with higher compactness, which lead to the accumulation of heat as well as higher LST during daytime. The ENN and CNI also showed similar relationships with DLST. ENN can be seen as a measure of road width and isolation of buildings, and the CNI is an important indicator for measuring direct solar radiation. Wider distances among buildings and higher ratios between buildings and road widths create a relative open building pattern, which accelerates the heat loss and generates more building shade. At night, the relationship turned to be opposite, high-rise buildings along the wide roads and the streets themselves serve as heat sources for warming the surrounding areas. Besides, the wide roads in Beijing's old city are mostly covered by the asphalt with a high specific heat capacity, which might release more heat compared with other road surfaces at night. SVF was much more correlated with DLST than NLST, because sky visibility is directly related to the solar radiation during daytime. After sunset, the SVF was not sensitive to the influence of buildings on LSTs.

Table 6. The diurnal and nocturnal correlation coefficients between configuration metrics and LST. Blue and orange suggest higher negative and positive correlations, respectively, while white colour indicates lower correlation.

	Daytime							Night						
	Jan 21	Mar 26	May 13	Aug 17	Sep 02	Oct 20	Dec 04	Jan 13	Apr 4	Aug 19	Sep 01	Oct 08	Nov 02	Dec 22
LPI	-0.5	-0.51	-0.52	-0.49	-0.49	-0.5	-0.53	0.13	0.28	0.12	0.07	0.22	0.26	0.15
SIEI	0.18	0.18	0.25	0.26	0.23	0.23	0.14	-0.04	-0.19	-0.04	-0.07	-0.14	-0.12	-0.03
SIDI	0.18	0.2	0.28	0.3	0.25	0.22	0.13	0.04	-0.17	-0.04	-0.01	-0.2	-0.08	-0.04
LSI	0.46	0.5	0.55	0.53	0.45	0.45	0.44	0.15	-0.24	-0.14	0.01	-0.37	-0.12	-0.04
LFI	0.67	0.71	0.59	0.53	0.66	0.66	0.65	-0.56	-0.62	-0.46	-0.43	-0.4	-0.65	-0.54
LDI	0.55	0.56	0.56	0.54	0.53	0.53	0.56	-0.14	-0.3	-0.15	-0.05	-0.24	-0.3	-0.21
COI	-0.69	-0.73	-0.61	-0.55	-0.66	-0.67	-0.65	0.54	0.61	0.43	0.39	0.42	0.65	0.5
ENN	-0.55	-0.62	-0.53	-0.46	-0.62	-0.55	-0.58	0.56	0.55	0.46	0.42	0.35	0.64	0.38
CNI	-0.34	-0.37	-0.21	-0.17	-0.34	-0.34	-0.33	0.6	0.44	0.31	0.42	0.15	0.53	0.42
SVF	-0.27	-0.33	-0.48	-0.50	-0.35	-0.28	-0.20	-0.40	0.07	0.08	-0.15	0.37	-0.07	-0.02

-1 0 +1

4.4. Relative importance of landscape metrics for the variations of LSTs

This study applied 20 landscape metrics to judge the spatiotemporal associations between urban buildings and LSTs. As multicollinearity might exist, it is difficult to determine which metric has a more dominant effect on the variation of LSTs. To this end, we analyzed the relative importance of 3D landscape metrics on affecting LSTs using RF (Fig. 5).

During daytime, NP, ENN, and LDI took a higher proportion than the other indicators, which indicated that the buildings number, compactness degree, and road width have more significant influence on DLST. An interesting finding was that the relative importance of building height decreased from January to August, and then increased. The change of height importance is basically consistent to the intensity of solar radiation. For SVF, the relative importance increased until August, and then decreased. Compared with the building height, the SVF is more sensitive to the direct solar radiation. During summer, the solar radiation is quite strong, which directly affects the spatial distribution of urban ground temperature. Although high buildings might be conducive to a decrease of LST through generating massive buildings shades, the influence is still relatively weak. At night, the relative importance of landscape metrics for LST variations did not show significant regularity, but the buildings number, height and road width in most months had higher contribution to NLST than others. Wider roads with asphalt cover, high buildings and large building numbers might act to store more heat during daytime and then release more after sunset.

The R^2 values between the regression results and LSTs indicated that the landscape metrics were more sensitive to the variations in LST during daytime than that at night. Over four seasons, at least 66.7% of variations in DLST can be explained by the regression model, while at most 67.8% of variations in NLST were explained by the landscape metrics. As for the temporal changes, the R^2 value in March during daytime was highest, approximately 82.1%, and the diurnal regression results during summer were relatively higher than that during autumn and winter. The nocturnal values decreased from January (67.8%) to early September (42.2%), and then increased, which indicated that the influence of buildings on LST at night was weak during summer.

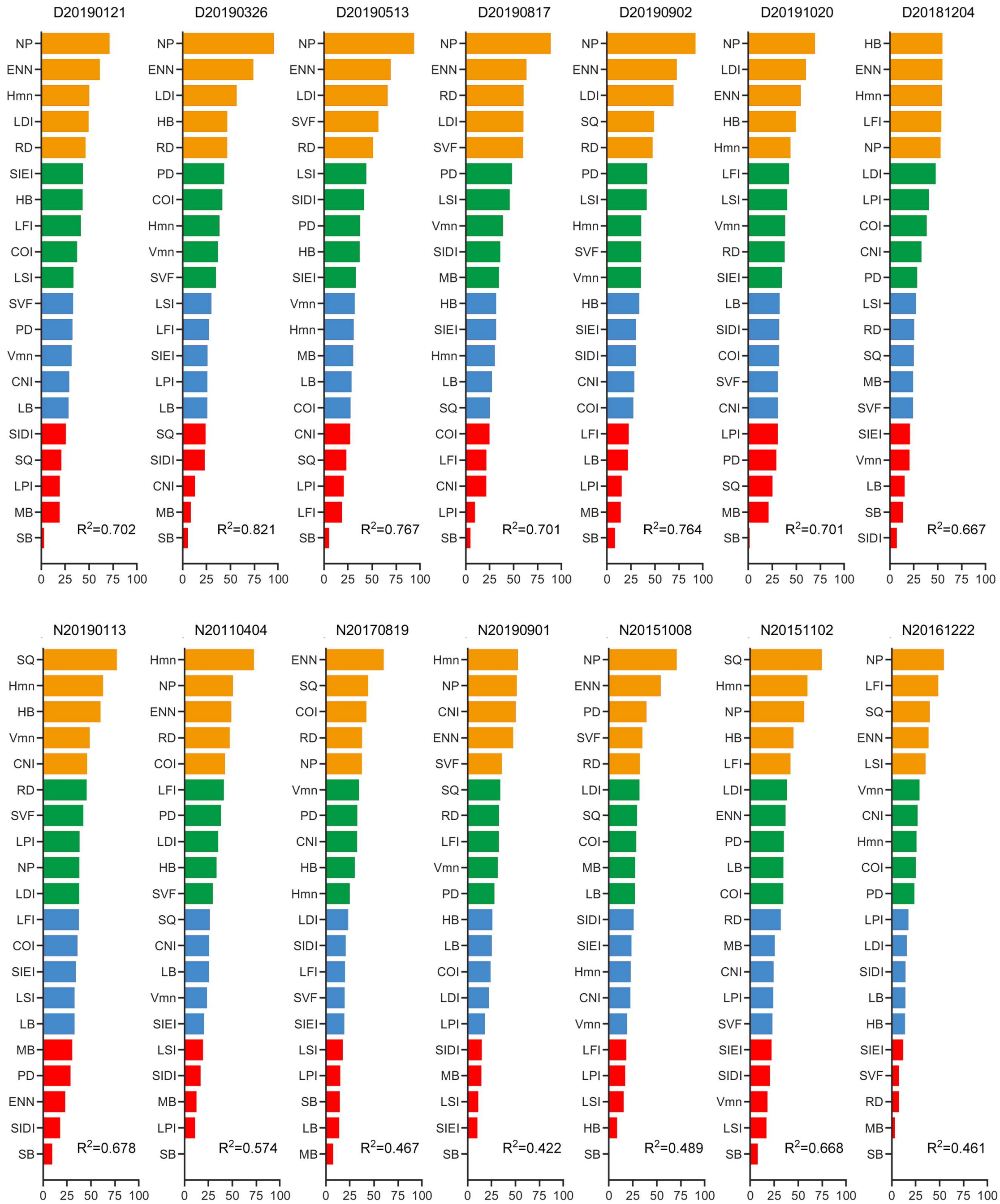

Fig. 5. The relative importance of 3D landscape metrics in the variations of LSTs over four seasons. The importance values tend to decrease with the colour changing from orange to red. The letter ‘D’ represents the daytime, ‘N’ represents the night, and the number represents the date of remote sensing images acquisition. For example, ‘D20190121’ represents the daytime LST on January 21, 2019.

5. Discussion

5.1. The efficiency of 3D landscape metrics measuring building patterns

Knowledge about how to measure building patterns in 3D space is a key for further monitoring of urban dynamics and its relationship with urban heat (Ng et al., 2012; Jhaldiyal et al., 2018; Kedron et al., 2019). Traditional methods mainly relied on the building's height, footprint and volume to describe the 3D building characteristics (Liu et al., 2017; Huang and Wang, 2019; Guo et al., 2020). These parameters aim at reflecting the horizontal and vertical information of single buildings, which are useful and simple but not sufficient. The influence of buildings on the urban heat environment is not a simple linear accumulation, but refers to the integrated effect of multiple factors, particularly the spatial arrangement of building patterns (e.g., open or compact pattern). Sky view factor (SVF) is another widely used parameter quantifying the extent of 3D open space, also taken as indicator for compactness of urban buildings (Guo et al., 2016; He et al., 2020; Yu et al., 2020). Chun and Guldmann (2014) applied SVF and other parameters to simulate the urban heat island in high-density central cities, but the influence of SVF on the LSTs is still uncertain and even contradictory. Positive, negative and insignificant relationships were all reported in previous studies (Hove et al., 2015; Berger et al., 2017; Huang and Wang, 2019). In this study, SVF was negatively correlated with the DLST, while the nocturnal relationship was not significant. The differences of SVF among multiple researches further proofed a complex relationship between urban morphology and LSTs, which can be hardly revealed by simple composition indices. Compared with traditional methods, 3D landscape metrics applied in this study can measure and compare the buildings characteristics targetedly and systematically. These metrics might suggest the degree of growth or sprawl of the built-up land in a city, which can be a useful tool that makes the research of relationships between building patterns and urban microclimate more convenient and comprehensive. Moreover, the composition and configuration metrics are related to socioeconomic phenomenon. For example, a compact buildings pattern with irregular spatial arrangement may affect the traffic congestion and lead to the increase of difficulties of old city planning and management through lock-in effect. More energy is likely to be consumed around high-rise buildings, who have less light accessibility and limit the growth of urban vegetation.

5.2. The sensitivity and relative importance of 3D landscape metrics indicating how building patterns affect LST

3D landscape metrics were the first time applied for the identification of the relationship between urban buildings and LSTs, and significant correlations were revealed for both composition and configuration metrics with DLST. During daytime, the magnitude of solar radiation is much higher than other heat sources, and the indirect influence of urban buildings on LSTs exceeds their direct influence. The proposed 3D landscape metrics can supply merits to measure the spatial component and structure characteristics of buildings, which affect the local LSTs by changing the light condition, atmospheric moisture and ventilation effect. As an example, the ENN in this study is seen as an indirect measure of road width. The wider road in the buildings pattern with open arrangement is a better ventilation path, more heat is removed and less solar radiation is absorbed with the assistance of urban green belt and buildings shade. The correlation coefficients of mean building height and building density with LSTs are over 0.6 in most months, indicating that an urban morphology of low building height, higher density and compact building yielded higher DLST level in old city.

At night, composition metrics were more sensitive to the LSTs, while the configuration metrics showed relatively weaker association. This is caused by the differences of ecological significance. The urban buildings affect the NLST mainly through running as heat resources, and composition metrics, such as buildings number, height and volume can be seen as indicators quantifying the heat release at night to a certain extent. The configuration metrics focusing the spatial structure hardly compare the heating ability among different buildings pattern. The fragmentation and segmentation degree of buildings pattern can be measured by the landscape division index and cohesion index. These buildings characteristics are possible to affect the spread path of heat released from the buildings, but hardly reflect the ability how buildings directly heat the surrounding area at night. Among the configuration metrics, some variations exist, and ENN were well associated with the surrounding temperature. CNI also showed similar relationship. These two metrics involves the reflection of road width and buildings height, which is directly related to heat release over the road and buildings. That's also the reason why the horizontal metrics among composition metrics were more sensitive to reveal the influence of buildings on the DLST, but the vertical metrics responded better to NLST.

The comparison between composition and configuration metrics through correlation coefficients is rough, and the linear analysis results might be affected by multicollinearity and nonlinearities in the data. In this context, random forest algorithm was applied to analyze the relative importance of buildings metrics for the variations of LSTs. The regression trees used in the random forest algorithm have the advantage that they can model complex relationships between predictor and response variables. The results showed that the R^2 during daytime exceed that at night significantly, indicating a better response of buildings characteristics to the variations of DLST than that of NLST. More buildings, narrow road and fragmented buildings pattern affect the surface reflection greatly, lead to a much worser ventilation effect and thermal dissipation capacity during daytime. At night, the buildings number, road width and buildings height had stronger influence on the LSTs than others in most months. These parameters can be seen as a measure of diurnal heat storage and nocturnal heat release ability. After daytime exposure to sunlight, high-rise buildings may store more heat compared with low-rise buildings, leading to more release at night. And the roads among the high-rise buildings are mostly paved with asphalt, which undoubtedly further contribute to the high temperature status of the surroundings.

5.3. Seasonal stability and variations of the relationship between buildings and LST

The relationship between urban building patterns and LSTs exhibited a quite stable behavior over four seasons, with the standard deviation of correlation coefficients lower than 0.05 for most of metrics across all date. This relatively consistent relationship was also revealed by other studies in different cities (Berger et al., 2017; Huang and Wang, 2019). Nevertheless, there were a few variations where the correlation coefficients during daytime in August were relatively lower than in other months. A similar phenomenon also existed at night, particularly among the configuration metrics, which indicated that stronger solar radiation and evapotranspiration of vegetation might cause weaker association between urban buildings and ground temperature in Beijing's old city. Such a conclusion still needs more verification in future, because the nocturnal data were collected from different years, which might have biased this study. Besides, the temporal variations of this relationship might vary with cities. Berger et al. (2017) analyzed how urban site characteristics affect LSTs over four seasons in Berlin and Cologne, where the results indicated a stronger association between urban buildings morphology and DLST during the summer. Huang and Wang (2019) found an increase in the magnitude of correlations between urban buildings and DLST in winter. The changing relationship over time might be not only related to the acquisition time of the remote sensing image, but also to the climate zones. Over different climate zones the solar radiation, building styles and urbanization are very different. More cities around the world might be considered to verify how the relationships change with climate zones over time, which can finally form a scientific basis for recommendations for urban planning and management.

5.4. Implications for historic city protection and urban planning

In Beijing's old historic city, the multiple styles of buildings are a synthetic product of urbanization, local historical culture and climate conditions. Since the modernization starting in mid-20th century and before 2008 Olympic Games, many courtyard houses and other traditional buildings gave way to modern buildings and public facilities to satisfy the entertainment needs and living requirements of urban residents. The historical and cultural values of traditional buildings were not questioned. The present study indicated that these buildings have their own special role in urban cooling, particularly at night. In addition to urban geometrical features, the materials of building envelopes and street paving also have an important influence on the LSTs. In contrast to the reinforced concrete structure of modern high-rise buildings, the envelope of traditional houses in the old city mainly consists of green bricks, grey tiles, and wood. Streets among traditional houses are usually covered by cement and green bricks, while modern buildings are mainly surrounded by asphalt roads. Differences in their specific heat capacity cause that the surface temperature over the latter increases slowly during daytime, but after sunset it releases more heat and yields a higher NLST level. The lower NLST in the low-rise regions supplies better environmental comfort compared with high-rise buildings. Temperature differences over the surface might cause air pressure differences between urban regions, which are conducive to wind formation, and thus play an important role in mitigating the nocturnal urban heat island. On the other hand, considering the high temperature zones mainly distributed in the low-rise buildings during daytime, targeted policies for old city planning and management should be considered to reduce the DLST in future together with the protection of historical old cities. Several suggestions are recommended based on our results:

- Planned demolition of some traditional houses is necessary for obtaining more regular and open building patterns. This measure is not haphazard demolition, but aims at improving ventilation and green spaces, which is also useful to avoid urban waterlogging.
- The roads among the traditional houses could be widened. In addition to improved ventilation paths, it is useful to avoid traffic congestion and reduce energy consumption as well as greenhouse gases emissions. Moreover, new pavement materials for heat loss and greenery covers along the street should be considered for facilitating the mitigation of high LSTs.
- The roofs of buildings can be covered by vegetation or water, if possible, more solar radiation absorption would be avoided. This makes communities more environmentally friendly and livability. Boston ivy can be planted on building walls to provide shade and absorb heat.
- For newly designed communities, an open arrangement is a good choice that has more green space improving the local urban heat environment and water cycle through evapotranspiration. Urban green infrastructure is an important

influencing factor maintaining physical and mental health of humans, particularly for the elderly and children.

These suggestions are derived from the application of our concept to this urban hotspot. An application to the heat management of other old towns should reevaluate them according to the location's peculiarities of terrain, climate and human environment. Actually, the thermal requirements of cities depend on their climate zones (Nichol and Wong, 2005; Berger et al., 2017; He et al., 2020). In cold regions, the heat accumulation within cities might be conducive to create a warm urban environment for the city dwellers, and can save a large amount of heating costs. But in tropical regions, higher LST levels might cause local abnormal airflow, air pollutants' accumulation, and the decrease of comfort of city dwellers. Therefore, how to guide and make good use of this special energy might be one key research topic with significant economic and environmental value for the sustainable development of cities.

5.5. Potential application of 3D landscape metrics and limitations

3D landscape metrics connecting urban morphology with urban heat might become a new paradigm for urban ecology. Rapid urbanization has led to the emergence of urban agglomerations consisting of a megacity and several neighboring cities. Such a combination of cities might influence the direction of the development of urban heat. A 3D landscape analysis not only can measure and compare the evolution of urban morphology, urban internal and external structures, but also can suggest effective indicators for monitoring these directional characteristics, and then help policy-makers searching for options to mitigate urban heat.

In addition to the limited acquisition times of remote sensing images, a deficiency of this study is that the proposed 3D metrics did not consider any directional characteristics of urban buildings and roads. The texture of the arrangement of buildings affects the LSTs significantly by changing the wind velocity. An isotropic building pattern in 3D space might decrease ventilation and heat dissipation capacity and then cause massive heat accumulation. A spectral analysis based on statistical autocorrelation might be a useful tool for further studies of the influence of texture characteristics of the built landscape on urban heat. Besides this, the size of the moving window measuring urban building patterns might have affected the relationship between urban morphology and LSTs, which actually refers to scale issues. Compared with the single correlation value under a given scale, multi-scale correlation characteristics may be more reliable and valuable for the identification of this relationship. In this study, the trees and greenery along streets and within buildings were not considered due to the lack of corresponding data sources. In the future, unmanned aerial vehicles with thermal infrared cameras might be used to create more precise 3D city data, including the urban green, which could be advantageous in studying the influence of varied urban site characteristics on LSTs.

6. Conclusions

Much research was been conducted over the past decade to understand how urban morphology affects urban heat, mostly focused on diurnal relationships and 2D building characteristics. Involving the urban 3D morphology, this study proposed a set of 3D landscape metrics that characterize the composition and configuration of urban buildings and were calculated from thermal infrared remote sensing images. From our results we conclude:

- The suggested 3D landscape metrics measure and systematically compare the buildings characteristics. The high-rise buildings have a higher degree of isolation, regularity and spatial aggregation, while the diversity, compactness and connectivity are larger in low-rise buildings.
- There are complex relationships between the 3D landscape metrics and the DLSTs and NLSTs. Local LSTs were significantly affected by the buildings design characteristics, such as buildings height, density and buildings styles. Higher building density, compact buildings pattern and irregular building arrangements yielded higher DLST, whereas the highest NLST occurred around modern high-rise buildings.
- The responses and sensitivities of 3D landscape metrics describing the diurnal and nocturnal impacts of urban morphology on LSTs differed obviously due to

the differences of ecological significance. Both composition and configuration metrics were highly correlated with DLSTs, but the composition metrics responded better to NLSTs than configuration metrics.

- DLST as well as NLST variations are significantly correlated with building numbers, road width, and fragmentation of buildings. The influence of building height on NLST was quite significant in most months. More buildings, narrow roads and fragmented buildings greatly affect the surface reflection, worsen the ventilation effect, and then cause massive accumulation of heat.
- The link between urban morphology and LSTs was fairly consistent over all four seasons. The summer relationship was weaker for both DLST and NLST, which might be caused by stronger solar radiation and evapotranspiration of urban vegetation.

Declaration of Competing Interest

The authors declare that they have no known competing financial interests or personal relationships that could have appeared to influence the work reported in this paper.

Acknowledgement

The first author would like to express his gratitude for the research support from China Scholarship Council under Grant No. 202008080124.

References

Berger, C., Rosentreter, J., Voltersen, M., Baumgart, C., Schmullius, C., &Hese, S. (2017). Spatio-temporal analysis of the relationship between 2D/3D urban site characteristics and land surface temperature. *Remote sensing of environment, 193,* 225-243. https://doi.org/10.1016/j.rse.2017.02.020

Chun, B., & Guldmann, J. M. (2014). Spatial statistical analysis and simulation of the urban heat island in high-density central cities. *Landscape and urban planning, 125,* 76-88. http://doi.org/10.1016/j.landurbplan.2014.01.016

Frazier, A. E., & Kedron, P. (2017). Comparing forest fragmentation in Eastern US forests using patch-mosaic and gradient surface models. *Ecological informatics, 41,* 108-115. http://doi.org/10.1016/j.ecoinf.2017.08.002

Frazier, A. E. (2019). Emerging trajectories for spatial pattern analysis in landscape ecology. *Landscape Ecology, 34*(9), 2073-2082. http://doi.org/10.1007/s10980-019-00880-1

Geros, V., Santamouris, M., Karatasou, S., Tsangrassoulis, A., & Papanikolaou, N. (2005). On the cooling potential of night ventilation techniques in the urban environment. Energy and Buildings, 37(3), 243-257. http://doi.org/10.1016/j.enbuild.2004.06.024

Gillespie, A., Rokugawa, S., Hook, S. J., Matsunaga, R., & Kahle, A. B. (1999). Temperature/emissivity separation algorithm theoretical basis document, version 2.4. *Nasa/Gsfc*, 1–64. http://eospso.gsfc.nasa.gov/sites/default/files/atbd/atbd-ast-05-08.pdf

Guo, A., Yang, J., Xiao, X., Xia, J., Jin, C., & Li, X. (2020). Influences of urban spatial form on urban heat island effects at the community level in China. *Sustainable Cities and Society, 53*. https://doi.org/10.1016/10.1016/j.scs.2019.101972

Guo, G., Zhou, X., Wu, Z., Xiao, R., & Chen, Y. (2016). Characterizing the impact of urban morphology heterogeneity on land surface temperature in Guangzhou, China. *Environmental modelling & software, 84*, 427-439.

https://doi.org/10.1016/j.envsoft.2016.06.021

He, B. J., Ding, L., & Prasad, D. (2020). Relationships among local-scale urban morphology, urban ventilation, urban heat island and outdoor thermal comfort under sea breeze influence. *Sustainable Cities and Society, 60*, 102289. https://doi.org/10.1016/j.scs.2020.102289

Hoechstetter, S., Walz, U., Dang, L. H., & Thinh, N. X. (2008). Effects of topography and surface roughness in analyses of landscape structure—a proposal to modify the existing set of landscape metrics. *Landscape Online, 3*(1), 1-14. https://doi.org/10.3097/LO.200803

Huang, X., & Wang, Y. (2019). Investigating the effects of 3D urban morphology on the surface urban heat island effect in urban functional zones by using high-resolution remote sensing data: A case study of Wuhan, Central China. *ISPRS Journal of Photogrammetry and Remote Sensing*, 152, 119-131. https://doi.org/10.1016/j.isprsjprs.2019.04.010

Hutengs, C., & Vohland, M. (2016). Downscaling land surface temperatures at regional scales with random forest regression. *Remote Sensing of Environment*, 178, 127-141. https://doi.org/10.1016/j.rse.2016.03.006

Jhaldiyal, A., Gupta, K., Kumar, P., & Thakur, P. (2018). Urban Climate Urban Morphology Extractor : A spatial tool for characterizing urban morphology. *Urban Climate, 24*, 237–246. https://doi.org/10.1016/j.uclim.2018.04.003

Jim, C. Y., & Chen, W. Y. (2010). External effects of neighbourhood parks and landscape elements on high-rise residential value. *Land Use Policy, 27*(2), 662-670. https://doi.org/10.1016/j.landusepol.2009.08.027

Jiménez-Muñoz, J. C., Sobrino, J. A., Skokovic, D., Mattar, C., & Cristobal, J. (2014). Land Surface Temperature Retrieval Methods From Landsat-8 Thermal Infrared Sensor Data. *IEEE Geoscience and Remote Sensing Letters, 11*(10), 1840-1843. https://doi.org/10.1109/LGRS.2014.2312032

Kedron, P. J., Frazier, A. E., Ovando-Montejo, G. A., & Wang, J. (2018). Surface metrics for landscape ecology: A comparison of landscape models across ecoregions and scales. *Landscape Ecology, 33*(9), 1489-1504. http://doi.org/10.1007/s10980-018-0685-1

Kedron, P., Zhao, Y., & Frazier, A. E. (2019). Three dimensional (3D) spatial metrics for objects. *Landscape Ecology, 34*(9), 2123-2132. http://doi.org/10.1007/s10980-019-00861-4

Li, Z., Tang, B., Wu, H., Ren, H., Yan, G., Wan, Z., ... & Sobrino, J. A. (2013). Satellite-derived land surface temperature: Current status and perspectives. *Remote Sensing of Environment,* 14-37. https://doi.org/10.1016/j.rse.2012.12.008

Liu, M., Hu, Y., & Li, C. (2017). Landscape metrics for three-dimensional urban building pattern recognition. *Applied Geography,* 66-72. https://doi.org/10.1016/j.apgeog.2017.07.011

Ma, Q., Wu, J., & He, C. (2016). A hierarchical analysis of the relationship between urban impervious surfaces and land surface temperatures: spatial scale dependence, temporal variations, and bioclimatic modulation. *Landscape ecology, 31*(5), 1139-1153. http://doi.org/10.1007/s10980-016-0356-z

McGarigal, K., Tagil, S., & Cushman, S. A. (2009). Surface metrics: an alternative to patch metrics for the quantification of landscape structure. *Landscape ecology, 24*(3), 433-450. http://doi.org/10.1007/s10980-009-9327-y

Ng, E., Chen, L., Wang, Y., & Yuan, C. (2012). A study on the cooling effects of greening in a high-density city: An experience from Hong Kong. *Building and environment, 47*, 256-271. https://doi.org/10.1016/j.buildenv.2011.07.014

Nichol, J., & Wong, M. S. (2005). Modeling urban environmental quality in a tropical city. *Landscape and urban planning, 73*(1), 49-58. http://doi.org/10.1016/j.landurbplan.2004.08.004

Nichol, J. (2005). Remote sensing of urban heat islands by day and night. *Photogrammetric Engineering & Remote Sensing, 71*(5), 613-621. https://doi.org/10.14358/PERS.71.5.613

Patz, J. A., Campbell-Lendrum, D., Holloway, T., & Foley, J. A. (2005). Impact of regional climate change on human health. *Nature, 438*(7066), 310. http://doi.org/10.1038/nature04188

Qin, Z., Karnieli, A., & Berliner, P. (2001). A mono-window algorithm for retrieving land surface temperature from Landsat TM data and its application to the Israel-Egypt border region. *International Journal of Remote Sensing, 22*(18), 3719-3746. https://doi.org/10.1080/01431160010006971

Salamanca, F., Georgescu, M., Mahalov, A., Moustaoui, M., & Wang, M. (2014). Anthropogenic heating of the urban environment due to air conditioning. *Journal of Geophysical Research, 119*(10), 5949-5965. https://doi.org/10.1002/2013JD021225

Tiangco, M., Lagmay, A. M., & Argete, J. (2008). ASTER-based study of the night-time urban heat island effect in Metro Manila. *Journal of remote sensing, 29*(10), 2799-2818. https://doi.org/10.1080/01431160701408360

United States Environmental Protection Agency (US EPA) Excessive Heat Events Guidebook U.S., Environmental Protection Agency, Washington, DC (2006)

Van Hove, L. W. A., Jacobs, C. M. J., Heusinkveld, B. G., Elbers, J. A., Van Driel, B. L., & Holtslag, A. A. M. (2015). Temporal and spatial variability of urban heat island and thermal comfort within the Rotterdam agglomeration. *Building and Environment*, 83, 91-103. https://doi.org/10.1016/j.buildenv.2014.08.029

Voogt, J. A., &Oke, T. R. (2003). Thermal remote sensing of urban climates. *Remote sensing of environment, 86*(3), 370-384. https://doi.org/10.1016/S0034-4257(03)00079-8

Wang, H., Zhang, Y., Tsou, J., & Li, Y. (2017). Surface urban heat island analysis of Shanghai (China) based on the change of land use and land cover. *Sustainability, 9*(9), 1538. http://doi.org/10.3390/su9091538

Wu, J. (2004). Effects of changing scale on landscape pattern analysis: scaling relations. *Landscape ecology, 19*(2), 125-138.

http://doi.org/10.1023/B:LAND.0000021711.40074.ae

Wu, Q., Guo, F., Li, H., & Kang, J. (2017). Measuring landscape pattern in three dimensional space. *Landscape and Urban Planning, 167,* 49-59. http://doi.org/10.1016/j.landurbplan.2017.05.022

Xu, J., Zhang, F., Jiang, H., Hu, H., Zhong, K., Jing, W., ... & Jia, B. (2020). Downscaling ASTER land surface temperature over urban areas with machine learning-based area-to-point regression Kriging. *Remote Sensing*, 12(7), 1082. https://doi.org/10.3390/rs12071082

Yu, S., Chen, Z., Yu, B., Wang, L., Wu, B., Wu, J., & Zhao, F. (2020). Exploring the relationship between 2D/3D landscape pattern and land surface temperature based on explainable eXtreme Gradient Boosting tree: A case study of Shanghai, China. *Science of the Total Environment, 725*, 138229. https://doi.org/10.1016/j.scitotenv.2020.138229